THE JOURNAL OF BIOLOGICAL CHEMISTRY VOL. 290, NO. 31, pp. 19067–19080, July 31, 2015

Redox-dependent Ligand Switching in a Sensory Heme-binding GAF Domain of the Cyanobacterium *Nostoc* sp. PCC7120*[S]

Received for publication, March 23, 2015, and in revised form, June 9, 2015 Published, JBC Papers in Press, June 10, 2015, DOI 10.1074/jbc.M115.654087

Kun Tang[‡§1], Markus Knipp[§¶], Bing-Bing Liu[‡], Nicholas Cox[§], Robert Stabel[§], Qi He[‡], Ming Zhou[‡2], Hugo Scheer[‖3], Kai-Hong Zhao[‡3,4], and Wolfgang Gärtner[§5]

From the [‡]State Key Laboratory of Agricultural Microbiology, Huazhong Agricultural University, Wuhan 430070, China, the [§]Max Planck Institute for Chemical Energy Conversion, Stiftstrasse 34-36, D-45470 Mülheim, Germany, [¶]Resolv, Faculty for Chemistry and Biochemistry, Ruhr University Bochum, D-44780 Bochum, Germany, and the [‖]Department of Biologie I, Ludwig-Maximilians-Universität, Menzinger Strasse 67, D-80638 München, Germany

Background: Three GAF domain proteins from cyanobacteria (*Nostoc* PCC7120) identified with heme group binding signatures.
Results: Protein All4978 composed of a heme-binding domain and a helix-turn-helix (HtH) motif switches ligands from cysteine (ferric state) to histidine (ferrous state) and binds DNA preferentially in ferric state.
Conclusion: The ligand-switch mechanism suggests redox-dependent signaling.
Significance: HtH activity regulation by a GAF-bound heme is novel for cyanobacteria.

The genome of the cyanobacterium *Nostoc* sp. PCC7120 carries three genes (*all4978, all7016,* and *alr7522*) encoding putative heme-binding GAF (cGMP-specific phosphodiesterases, adenylyl cyclases, and FhlA) proteins that were annotated as transcriptional regulators. They are composed of an N-terminal cofactor domain and a C-terminal helix-turn-helix motif. All4978 showed the highest affinity for protoheme binding. The heme binding capability of All7016 was moderate, and Alr7522 did not bind heme at all. The "as isolated" form of All4978, identified by Soret band (λ_{max} = 427 nm), was assigned by electronic absorption, EPR, and resonance Raman spectroscopy as a hexacoordinated low spin Fe^{III} heme with a distal cysteine ligand (absorption of δ-band around 360 nm). The protoheme cofactor is noncovalently incorporated. Reduction of the heme could be accomplished by chemically using sodium dithionite and electrospectrochemically; this latter method yielded remarkably low midpoint potentials of −445 and −453 mV (following Soret and α-band absorption changes, respectively). The reduced form of the heme (Fe^{II} state) binds both NO and CO. Cysteine coordination of the as isolated Fe^{III} protein is unambiguous, but interestingly, the reduced heme instead displays spectral features indicative of histidine coordination. Cys-His ligand switches have been reported as putative signaling mechanisms in other heme-binding proteins; however, these novel cyanobacterial proteins are the first where such a ligand-switch mechanism has been observed in a GAF domain. DNA binding of the helix-turn-helix domain was investigated using a DNA sequence motif from its own promoter region. Formation of a protein-DNA complex preferentially formed in ferric state of the protein.

Hemes,[6] in particular protoheme, are ubiquitous and essential protein cofactors for many biological reaction pathways (1–4). Nature has evolved quite variable protein folds competent for heme incorporation, in a covalent or noncovalent manner. The most apparent one from mankind's point of view is the globin fold. However, many other protein domains bind hemes, modifying the chemical activity of the heme cofactor by the surrounding protein, thereby rendering it a redox-active component (5) or a gas sensor (6), for example. For these two functionalities, the heme-binding proteins (or protein domains) act as regulatory or signaling systems, allowing the organism to acclimate to changing environmental conditions.

A relatively large group of heme binding-proteins have a PAS (Per, period circadian protein, Arnt, aryl hydrocarbon receptor nuclear translocator protein, Sim, single-minded protein) domain. Others, such as nitrophorins (7), adopt the lipocalin structure. Only a few proteins have been described as binding

* This work was supported in part by the Max-Planck-Society and the Cluster of Excellence RESOLV (EXC 1069) funded by the Deutsche Forschungsgemeinschaft. The authors declare that they have no conflicts of interest with the contents of this article.
[S] This article contains supplemental Table S1.
[1] Recipient of a grant from the China Scholar Council.
[2] Recipient of Grant 31370777 from the National Natural Science Foundation of China.
[3] Recipient of National Natural Science Foundation of China Grant 31110103912.
[4] Recipient of National Natural Science Foundation of China Grants 31270893 and 21472055. To whom correspondence may be addressed: State Key Laboratory of Agricultural Microbiology, Huazhong Agricultural University, Wuhan 430070, China. E-mail: khzhao@163.com.
[5] Supported by the Max-Planck-Society. To whom correspondence may be addressed: Max Planck Institute for Chemical Energy Conversion, Stiftstr. 34-36, 45470 Mülheim, Germany. Tel.: 49-208-306-3693. E-mail: wolfgang.gaertner@cec.mpg.de.

[6] The abbreviations used are: heme, protoheme; 5c, 5-coordinate; 6c, 6-coordinate; HS, high spin; HtH, helix-turn-helix; IMAC, immobilized metal affinity chromatography; LS, low spin; MCD, magnetic circular dichroism; P450, cytochrome P450; P420, cytochrome P420; PDB, Protein Data Bank; aa, amino acid; BisTris, 2-[bis(2-hydroxyethyl)amino]-2-(hydroxymethyl)propane-1,3-diol; RR, resonance Raman; SHE, standard hydrogen electrode.

the heme cofactor in a GAF (cGMP-specific phosphodiesterases, adenylyl cyclase, and FhlA) domain (8, 9). The lipocalin motif is noticeable for its eight-stranded β-barrel structure, whereas PAS and GAF domains, despite a low sequence homology, share a similar structural topology of a five-stranded antiparallel β-sheet arrangement connected by surrounding α-helices, forming the ligand binding pocket (8, 10).

There are relatively few examples of proteins that contain a heme-binding GAF domain as follows: MA4561 from *Methanosarcina acetivorans* (11) and DosS (sometimes designated DevS) and DosT from *Mycobacterium tuberculosis*, which have been proposed as redox and gas sensors (5, 9). DosS and DosT are both tandem GAF domain proteins, where in both proteins, the N-terminal GAF domain, termed GAF_{DosS} and GAF_{DosT}, respectively, bind a heme (5, 9, 12, 13). Signaling in these proteins is accomplished through a histidine kinase, located downstream of the second GAF domain. Both proteins coordinate the heme iron via a histidine residue (9, 10). However, although GAF_{DosS} and GAF_{DosT} share 75% amino acid sequence identity (14), each was assigned a different sensory function; both proteins are capable of binding gas molecules such as CO and NO in the ferrous oxidation state; however, only GAF_{DosT} forms a stable complex with O_2, whereas GAF_{DosS} instead is oxidized to form the ferric complex (5). The binding of CO and NO to GAF_{DosS} has little effect on the histidine kinase activity, but the change of the iron oxidation state does affect its activity remarkably, suggesting GAF_{DosS} represents a redox sensory domain (15). In contrast, the ferrous oxidation state of GAF_{DosT} is very stable, with the histidine kinase activity instead modulated by the concentration of the coordinating gas molecule, indicating a gas sensory function of GAF_{DosT} (5). A similar GAF domain has been recently described for the histidine kinase MA4561 from *M. acetivorans*, termed GAF_{heme}. Its heme iron is also likely coordinated by a histidine residue (11). However, in contrast to the *b*-type heme of GAF_{DosS} and GAF_{DosT}, the heme in MA4561 is covalently attached via a Cys side chain. The function of this domain is still under investigation; however, there is evidence that the GAF_{heme} from *M. acetivorans* might be involved in (di)methyl sulfide metabolism.

A recent survey of cyanobacterial genomes (16) identified PAS domains assigned as potential heme-binding domains. GAF domains with a corresponding heme-binding function have so far not been reported in cyanobacteria. GAF domains, with tetrapyrrole ligand-binding capacity, are most prominent in canonical phytochromes, red-/far red-sensing photoreceptors present in both plants and bacteria (17), and in the related cyanobacteriochromes (16). In these chromoproteins, a cysteine residue in the GAF domain facilitates covalent binding of the chromophore, an open-chain tetrapyrrole (bilin) derivative, to the protein scaffold, which undergoes light-driven photochromic conversion between a resting and a signaling state.

Here, we report three genes (*all4978, all7016* and *alr7522*) from *Nostoc* sp. PCC7120 all of which encode GAF domain proteins that show signatures for heme-binding sites. Annotation of the genome identifies them as transcriptional regulators based on a C-terminally located helix-turn-helix (HtH) domain of the LuxR type (Fig. 1) (18). The gene products were heterologously expressed, purified to homogeneity, and spectrally characterized. The highest loading of the heme was found for All4978. Moderate loading was found for All7016, and Alr7522 did not bind heme at all. In contrast to the heme-binding GAF domains from *M. acetivorans* and *M. tuberculosis* described above, which carry a histidine kinase as a signaling domain, the three GAF domain proteins from *Nostoc* carry an HtH motif at their C-terminal end. These proteins from *Nostoc* represent the first examples where a heme-binding GAF domain is combined, putatively in a regulatory fashion, with an HtH structural motif.

Experimental Procedures

Cloning and Protein Preparation—DNA encoding full-length proteins and the GAF domains of All4978, All7016, and Alr7522 were PCR-amplified from genomic DNA of *Nostoc* sp. PCC7120 and cloned into pET vectors, thereby furnishing the recombinant proteins with His tags allowing for facile affinity purification. Details can be found in supplemental Table S1. Besides the wild-type proteins, for $GAF_{All4978}$ the following site-directed mutations were generated: Y41F/Y41G, C92S/C92G, H95A/H95G, H97A/H97G, H99A, and C138S (Table 1 and supplemental Table S1). For the expression of all proteins, transformed *Escherichia coli* BL21 cells (DE3) were grown in LB medium at 37 °C and 200 rpm to $OD_{600\ nm} = 0.8$, at which time the cells were induced by addition of 1 mM isopropyl β-D-thiogalactopyranoside. Growth was continued for 14 h at 18 °C. For all further experiments, wild-type and mutated $GAF_{All4978}$ showing the highest loading with heme were employed.

To improve the heme/protein ratio, hemin (Sigma) was added in some experiments before induction (10 mg/ml in 0.1 M NaOH per 1 liter of culture) (12). Wild-type and mutated proteins were purified as described (19). Harvested cells were lysed, and the supernatant after centrifugation was loaded onto an IMAC column. After elution from the affinity column, protein was dialyzed against a potassium phosphate buffer, KP_i (20 mM, pH 7.5), containing 50 mM NaCl and 5 mM EDTA, loaded onto an ion exchange column (HiPrep DEAE-FF 16/10, GE Healthcare), and eluted at a flow rate of 1 ml/min with the same buffer and a linear 10 mM NaCl/min gradient to remove most of the non-heme-loaded apoprotein. Such purified proteins were then concentrated for further studies. The purity of the proteins was confirmed by SDS-PAGE (4–12% BisTris Gel, Novex).

Electronic Absorption Spectroscopy—Absorption spectra of protein solutions (~5 μM in phosphate buffer, see above) were recorded at room temperature in 1-cm quartz cuvettes (UV-2401 spectrophotometer, Shimadzu). For ferrous compounds, a gas-tight cuvette was used that was purged thoroughly with N_2 or CO prior to the addition of reductants.

Butanone Extraction (20)—800 μl of 2-butanone and 200 μl of 1 M HCl were added to a sample of 2 ml of $GAF_{All4978}$. The mixture was gently vortexed and kept for several minutes. Noncovalently bound heme was found in the upper organic phase, whereas covalently bound heme remains in the lower aqueous phase.

Pyridine Hemochrome Assay—The pyridine hemochrome assay was carried out as described (21). In detail, 0.5 ml of protein solution was mixed with 0.5 ml of 200 mM NaOH, 40% (v/v)

pyridine, and 3 μl of 0.1 M of $K_3Fe(CN)_6$. Upon measurement of its UV-visible spectrum (600–400 nm), several crystals of $Na_2S_2O_4$ (2–5 mg) were added, and the UV-visible spectrum was recorded again.

Spectroelectrochemical titrations were carried out using an SEC-C spectroelectrochemical cell (1-mm light path) equipped with a platinum gauze working electrode and a platinum counter-electrode (ALS Co., Ltd., Japan) at room temperature. A silver/AgCl reference electrode (E° = −205 mV *versus* SHE) was attached (BASi, Inc.). Protein samples were rendered essentially O_2-free through dialysis (nominal molecular mass limit of 12–14 kDa) in KP_i in an anaerobic chamber. Methyl viologen, anthraquinone-2-sulfonic acid, and $Ru(NH_3)_6Cl_3$ were added as electrochemical mediators at ~20 μM concentrations (22, 23). The electrochemical potential, E_{appl}, was controlled by an ϵ potentiostat (BASi, Inc.). Initially, E_{appl} was set to −545 mV *versus* SHE and then increased by steps of 20 mV, whereas absorbance spectra were collected between 600 and 300 nm upon equilibration with a Cary 50 spectrophotometer.

Chemical Reduction—Reduction of $GAF_{All4978}$ was performed by the addition of a freshly prepared $Na_2S_2O_4$ solution (1 mM in water) in a glove box in an N_2/H_2 (98:2) atmosphere. Spectra between 600 and 300 nm were recorded every 3 s with a Cary 50 spectrophotometer that was connected via fiber optics with the cuvette holder inside the glove box. The experiment was repeated with mixtures of 1 mM $Na_2S_2O_4$ in the presence of 5 mM ascorbic acid, 5 mM glutathione (GSH), 2 μM flavine mononucleotide (FMN), 2 μM flavine adenine dinucleotide (FAD), or 100 μM nicotinamide adenine dinucleotide (NADH) (15).

Magnetic Circular Dichroism Spectroscopy (MCD)—MCD measurements were performed at room temperature using a JASCO (Model J-715) spectropolarimeter equipped with a 1.4 tesla permanent magnet (Olis) in quartz cuvettes with 1 cm path length. Four spectra were accumulated between 300 and 700 nm for each sample with the longitudinal magnetic field in direction of, or opposite to the light beam ($\pm B$). The respective baseline spectra were subtracted before further processing. Because the observed spectra are a combination of the CD and the MCD signals ($\Delta A_{obs}(\pm B) = \Delta A_{CD} \pm \Delta A_{MCD}$), pure MCD spectra were calculated as shown in Equation 1,

$$\Delta A_{MCD} = \frac{\Delta A_{obs}(+B) - \Delta A_{obs}(-B)}{2} \qquad \text{(Eq. 1)}$$

Resonance Raman Spectroscopy—Samples of ~50 μM protein were generally used. Anaerobic samples were prepared in an anaerobic chamber (N_2/H_2 (98:2) atmosphere) furnished with palladium catalysts. Reduction was performed by the addition of $Na_2S_2O_4$ and was followed spectrophotometrically. Samples were transferred to quartz tubes (3.8 mm diameter) connected to a valve. CO was added by flushing of the septum-closed sample with CO gas. NO was added by the addition of diethylammonium 2-(*N*,*N*-diethylamino)-diazenolate-2-oxide (Enzo Life Science) in 2–3-fold excess. After freezing of the solution in liquid N_2, the tubes were sealed under vacuum by glass melting.

Resonance Raman (RR) spectra were recorded with a scanning double monochromator. The excitation line at 406.7 nm was provided by a coherent K-2 Kr^+ ion laser, and the sample was rotated throughout the measurement to minimize radiation damage. For measurements in frozen solution, samples of ~50 μM were filled into 3-mm quartz tubes and kept in a quartz Dewar filled with liquid N_2 during the measurement.

FTIR Spectroscopy—The degassed protein solution was saturated with CO before being reduced under controlled conditions with $Na_2S_2O_4$ in an anaerobic chamber. Samples were transferred under anaerobic conditions to a 50-μl gas-tight transmission cell (pathlength, 50 μm) equipped with CaF_2 windows with 2 cm^{-1} resolution. FTIR spectra were recorded on a Bruker IFS 66v/S FTIR spectrometer equipped with an MCT photo-conductive detector and a KBr beam splitter. The temperature was set to 25 °C with a thermostat (RML, LAUDA).

EPR Spectroscopy—X-band EPR measurements were performed at 6–25 K using a Bruker E500 spectrometer, equipped with an Oxford Instruments ESR 935 cryostat and ITC4 temperature controller. Experimental parameters were as follows: ν_{mw} = 9.65 GHz; P_{mw} = 0.2–20 milliwatts; modulation amplitude = 1 millitesla, and modulation frequency 100 kHz. Spectra were fitted as a single S = ½ species with rhombic g-tensor, consistent with low spin Fe^{III} iron signals. Spectral simulations were performed numerically using the EasySpin package (24) in MATLAB. An isotropic line width of 3 millitesla was used.

Homology Modeling—Homology modeling was performed with the SWISS-MODEL server (25–27) using the PDB files of DosS and DosT (2W3G and 2VZW) as templates. Refinement was performed with the Swiss-PDBViewer version 4.1 (28) using the GROMOS96 (29) implementation for local energy minimizations. Modeling results were evaluated by What_Check (30) and Procheck (31).

Electrophoretic Mobility Shift Analysis—The digoxigenin gel shift kit (2nd Generation, Roche Applied Science) was used for all DNA binding tests. For DNA binding tests, a 25-bp double-stranded oligonucleotide from the *all4978* promoter region (forward, 5′-GCTGGTATTAGCATAGAAGTAATTG-3′, and reverse, 5′-CAATTACTTCTATGCTAATACCAGC-3′) was synthesized (Metabion International AG) and labeled at both ends with digoxigenin. Full-length All4978 protein (N-terminally His-tagged) was purified as described previously. For control experiments, protein EL222 together with its DNA target (65) were used under identical conditions as described for All4978. The GAF domain of All4978 alone (no binding capacity due to removed HtH motif) was used under the same experimental conditions as described for the full-length protein. 15 nM DNA probes were incubated with different concentrations of the purified protein for 30 min at room temperature, in 50 mM Tris-HCl, pH 8.0, 100 mM NaCl, 5% glycerol. The mixtures were then loaded onto a 10% TBE gel (Invitrogen) at 4 °C in 0.5× TBE buffer (89 mM Tris-HCl, pH 8.0, 89 mM borate, and 2 mM EDTA). For the control experiment using unlabeled DNA and in the experiments described above, 150 nM unlabeled DNA was added. Gel running, transfer, and imaging were done as described by the manufacturer; gels were scanned with an LAS-4000 imager (Fuji film). When reducing conditions were required, fresh dithionite solution (5 mM final concentration) was added to all of the buffers and reaction mixtures.

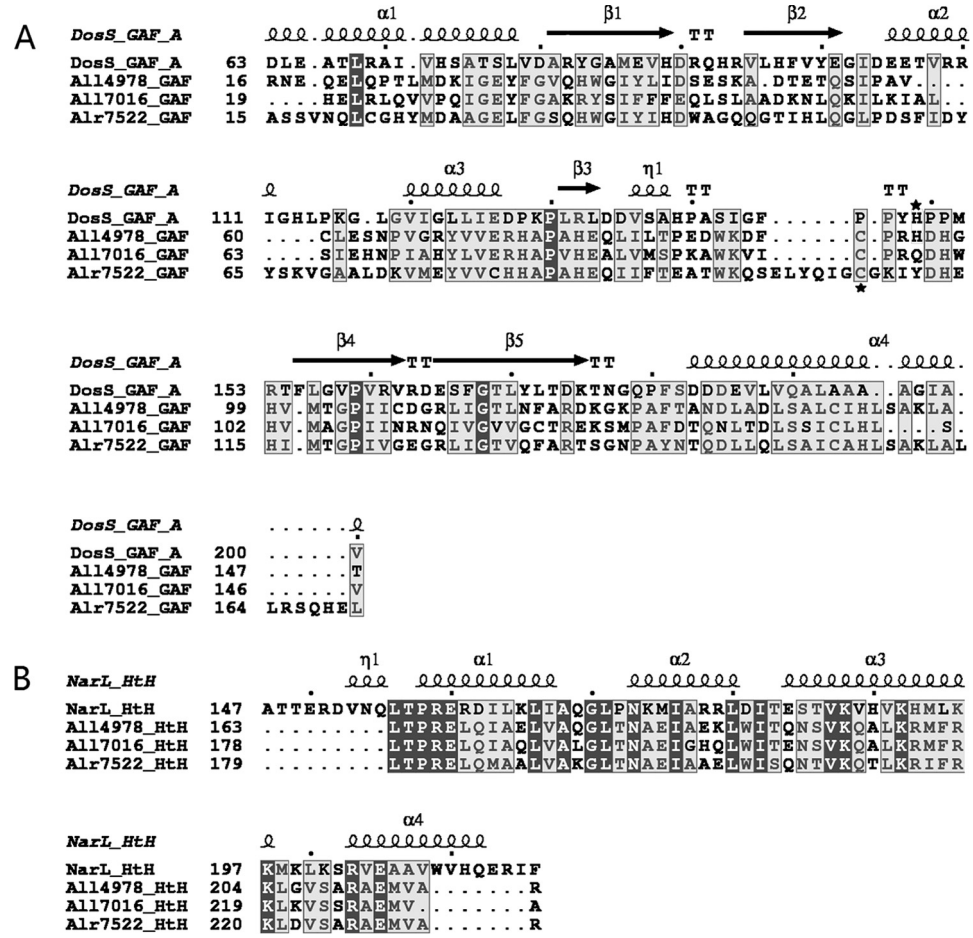

FIGURE 1. *A*, amino acid sequence alignment between GAF domains: $GAF_{All4978}$, $GAF_{All7016}$, $GAF_{Alr7522}$, and GAF_{DosS}. Secondary structure elements were derived from the x-ray structure of GAF_{DosS} (PDB code 2W3G). The proximal heme ligand His-149 of GAF_{DosS} and the potential proximal heme ligands for $GAF_{All4978}$, Cys-92 and His-95, are shown by *stars*. *B*, amino acid sequence alignment between helix-turn-helix motifs: $HtH_{All4978}$, $HtH_{All7016}$, $HtH_{Alr7522}$, and HtH_{NarL}. Secondary structure elements were derived from the x-ray structure of HtH_{NarL} (PDB code 1JE8). The C-terminally HtH domain of All4978 is highly similar to NarL of *E. coli* (PDB code 1JE8), nitrate reductase, an important enzyme to nitrogen metabolism. In NarL, the regulation proceeds via phosphorylation of a Rec domain (N-terminal, aa 10–124), followed by structural changes of the C-terminal HtH domain. Multiple alignment was done using the T-coffee software and visualized using ESPript.

Results

Structural, Absorbance, and Magnetic Properties of "As Isolated" $GAF_{All4978}$—All4978 encodes a protein of 224 amino acids that, according to protein domain prediction programs, is composed of two domains, an N-terminal GAF part (aa 17–147) and a C-terminally located HtH motif (aa 163–216). Most experiments on All4978 were performed with a construct ($GAF_{All4978}$) containing the GAF domain and short N- and C-terminal extensions (positions 1–170) plus an N-terminal His_6 tag. All7016 (aa 255 as full-length protein) contained the same structural elements as follows: an N-terminal GAF domain (aa 19–146) and a C-terminal HtH motif (aa 178–230). Expression products covering aa 4–168 and aa 1–173 were used as $GAF_{All7016}$ and $GAF_{Alr7522}$ in this study, respectively. The full-length protein and also the GAF domain expressed separately form dimers, as determined by gel filtration chromatography irrespective of the oxidation state (data not shown).

A survey for other heme-binding GAF domains identified DosS from *M. tuberculosis* as the structurally closest neighbor in current literature (also see under "Homology Modeling"). Despite the structural homology of these two proteins, a sequence alignment revealed only a moderate similarity between the two proteins (Fig. 1). In DosS, the proximal ligand to the heme iron was identified as His-149 (15). For the corresponding region of $GAF_{All4978}$, sequence alignment revealed an interesting pattern of three alternate histidine residues at positions 95–99 (HDHGH), preceded by a cysteine at position 92 (in DosS, the corresponding position is occupied by Pro-146). To determine whether a histidine residue serves also as proximal ligand to the heme in $GAF_{All4978}$, each of the three histidines was individually mutated.

Upon IMAC purification of the heterologously expressed protein in standard LB medium, the red-colored $GAF_{All4978}$ exhibits an absorbance spectrum typical of a heme protein (Fig. 2). Spectra of full-length protein and the separately expressed GAF domain are qualitatively identical; quantitatively they differ by an increased pigment-to-protein ratio (A_{427}/A_{280}) of the latter as a consequence of its shorter protein chain. Recombinant expression of full-length All4978 or $GAF_{All4978}$ in the presence of 5-aminolevulinic acid (1 mM) or hemin (5 μM) resulted in only a minor (~10%) increase of the pigment-to-protein ratio. Similarly, the addition of heme to the purified protein did

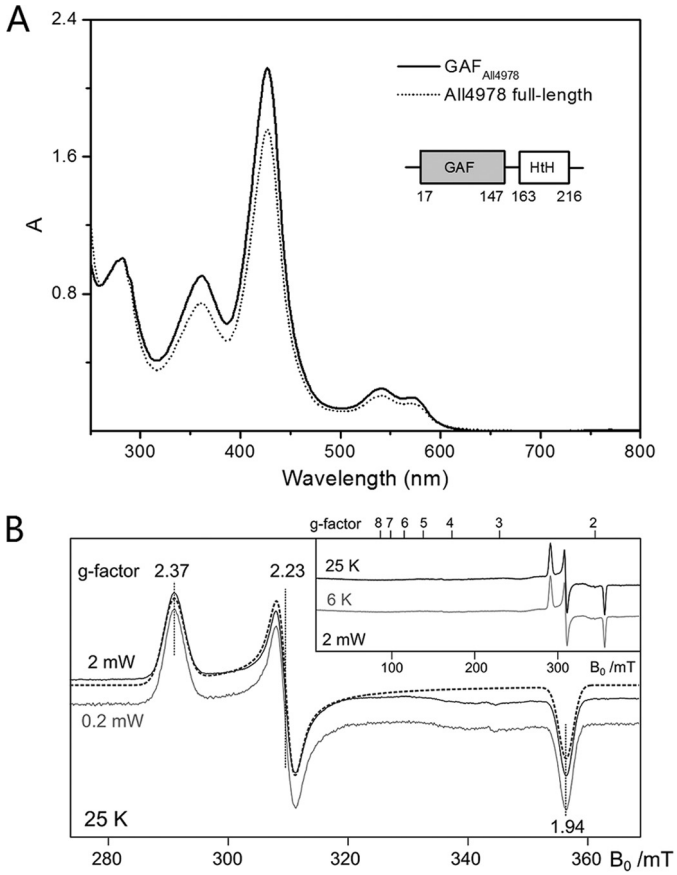

FIGURE 2. *A,* absorbance spectra and domain structure of as isolated heme-binding full-length All4978 and the separated GAF domain ($GAF_{All4978}$) from *Nostoc* sp. PCC 7120. *B,* corresponding low temperature X-band EPR spectra (9.65 GHz) of the as isolated $GAF_{All4978}$ collected for two microwave power (MP) values, 2 milliwatts (*black*) and 0.2 milliwatts (*gray*). The data traces were scaled to account for the difference in MP, *i.e.* multiplied by $\sqrt{MP}$. The *dashed line* shows a spin Hamiltonian simulation consistent with a low spin ($S = {}^1/_2$) Fe^{III} ferriheme signal. The *inset* shows that the ferriheme signal displays the same line shape over a large temperature range and demonstrated that the protein does not display any other EPR active species, *e.g.* high spin heme signals.

not further improve this ratio. Hemin incorporation by *E. coli* is not necessarily an efficient process, whereas supplementation of the medium by 5-aminolevulinic acid is known to improve heme biosynthesis. We thus consider the obtained ratio of A_{427}/A_{280} ~2 the maximal heme loading of the protein. Thus, it can be concluded that maximal heme loading of the protein was achieved. In contrast, heme loading in the GAF domain of All7016 could be significantly improved (~5-fold) by addition of hemin either during expression or to the crude lysate. Heme extraction, performed for the All4978 proteins, using organic solvents demonstrated noncovalent incorporation of the cofactor and identified it as a *b*-type heme, with mass spectrometric and HPLC analysis confirming noncovalent binding (data not shown). The molar extinction coefficient of the protein-cofactor complex was determined as $\epsilon = 183{,}000\ M^{-1}\ cm^{-1}$ at 427 nm, using a standard assay (21). This value was used for all further protein and cofactor quantifications. As most GAF domain proteins in cyanobacteria with the capability to incorporate a cofactor are found in bilin-binding phytochromes and related proteins, All4978 was screened for bilin binding under *in vivo* and *in vitro* conditions; however, no spectral indications of incorporation of the bilin cofactor could be found.

The electronic absorbance spectrum of the as isolated protein is characterized by sharp α- and β-bands at 571 and 540 nm, respectively, indicative of a low spin (LS) Fe^{III} ($S = ½$) (Fig. 2*A* and Table 1). A Soret band at 427 nm and a prominent δ-band at 360 nm are also clearly visible, characteristic of thiolate heme ligands (32, 33). Commensurate EPR measurements on the as isolated protein identified a single EPR active species centered about g ≈2 (Fig. 2*B*). The EPR signal displays fast magnetic relaxation as evidenced by the high microwave flux that can be used to measure the signal at cryogenic temperatures (<30 K) without significant power saturation ($P_{½}$ >2 milliwatts at 25 K); as shown in Fig. 2*B*, the magnitude of the EPR signal is the same using two microwave fluxes, 0.2 and 2 milliwatts, after accounting for the expected microwave power dependence. The intensity of the signal shows a linear dependence with the reciprocal of the measurement temperature (Fig. 2*B, inset*). Both of these properties are consistent with assigning the EPR signal to a single $S = ½$ species. No additional EPR signal was observed at low magnetic fields where high spin heme iron signals can be observed.

The line shape of the EPR signal is characteristic of a LS ferriheme. Such species typically display a rhombic EPR spectrum (three inflection points), with at least one turning point greater than g = 2 and one turning point less than g = 2. The relatively narrow width (g spread) of the EPR signal is indicative of a thiolate-coordinated heme (P-type). The fitted g values [2.37, 2.23, 1.92] are very similar to that seen for the heme cofactor of $P450_{cam}$ [2.41, 2.25, 1.91], which is coordinated by a thiolate residue and a water (for tabulated values see Walker (76)). Using these g values, estimates for the ligand field parameters can be deduced as follows: the tetrahedral (Δ/λ) and the rhombic splitting ($|V/\Delta|$), where V and Δ describe the energy level splittings of the occupied t_{2g} orbitals (d_{xz}, d_{xy}, and d_{yz}), and λ indicates the spin-orbit coupling. Using the "proper" axis system ($|V/\Delta| \leq ⅔$) as defined by Taylor (34), these g values yield $\Delta/\lambda = -5.37$ and ($|V/\Delta| = 0.40$, and constrain g_Z to lie in the plane of the heme ring. The strong similarity of these values to that of $P450_{cam}$ suggests the redox potential of $GAF_{All4978}$ and $P450_{cam}$ is likely to be similar.

The addition of strong ligands to ferric heme, such as imidazole, NO, and CN^-, did not change the absorbance spectrum suggesting that the distal site of the heme iron is either coordinated by a ligand residue (hexa-coordinated form) or its open coordination site is sterically shielded by the surrounding protein pocket. As indicated above, EPR data would suggest that if the ferric heme was hexa-coordinated, the 6th ligand would be water.

The as isolated protein (λ_{max} = 427 nm), characterized by EPR and by Raman as an Fe^{III} species, has been treated by $K_3[Fe(CN)_6]$, which caused a shift of the Soret band to 412 nm. Reduction of the as isolated protein by $Na_2S_2O_4$ led to an upshift of the 427-nm Soret band to 424 nm and a gain in intensity, concomitant with a concurrent change of the line shape of the α- and β-bands (Fig. 3 and Table 1). Exposure of the sample to air by opening the cuvette yielded rapid re-oxidation of the heme cofactor once $S_2O_4^{2-}$ was consumed, again generating,

TABLE 1

Absorption maxima (nm) of $GAF_{All4978}$ species for the α-, β-, and δ- and Soret bands in the as isolated proteins and the α- and β- and Soret bands in the ferrous state for the WT protein and the site-directed mutants, together with the heme contents relative to the WT protein (pH 7.5, 25 °C)

	As isolated					Reduced		
$GAF_{All4978}$	δ	Soret	α	β	Heme content[a]	Soret	α	β
WT	360	427	570	541	1	424	559	538
Fe^{II}–CO					1	420	568	539
Fe^{II}–NO					1	420		538
Y41G	360	426	571	540	0.51	425	558	529
Y41F	360	426	571	541	0.75	425	558	529
C92S		411			0.11	419	553	
C92G		412			0.06	420	553	528
H95A	360	426	567	541	0.46	425	557	530
H95G	360	425	570	540	0.37	424	557	528
D96A		423		536	0.18	424	558	528
H97A		417	563	531	0.12	422	556	528
H97G		417[b]			0.09	424	558	525
H99A		421		532	0.10	424	558	528
C138S	360	427	570	541	0.60	424	559	538

[a] Ratio between the heme absorption (Soret band) of mutant and WT after normalizing to the protein absorption at 280 nm is shown.
[b] This mutation led to a very unstable heme binding.

with a slightly shifted absorbance, the short wavelength form (λ_{max} = 413 nm). This reduced, re-oxidized sample showed the same Raman spectrum as the as isolated protein (see below), confirming its Fe^{III} state. The reduction experiment was performed over a pH range from 5.5 to 10 without any significant change of the spectral properties. When kept under reducing conditions, the addition of CO resulted in a significant change of the absorbance spectrum: the Soret band and the α- and β-bands downshifted to 420, 568, and 539 nm, respectively, indicating that, in contrast to the ferriheme state, the reduced heme does bind CO and, as identified in a separate experiment, also NO (Fig. 3). Similar effects were observed for the addition of NO and CO to the reduced $GAF_{All7016}$ domain (data not shown) unambiguously demonstrating that these novel heme-GAF domains in their reduced form bind these diatomic gas molecules. Homology modeling (see below) suggested a functional involvement of tyrosine 41 in the gas binding capacity. We thus mutated this residue into phenylalanine and glycine and repeated the CO-binding experiment. Also, electrochemical reduction was performed with these mutants. Spectra of CO-loaded wild-type and Y41F/Y41G mutants are virtually identical, and also the reduction experiment yielded potentials as found for the wild-type protein, excluding a functional role of Tyr-41 in the gas binding capacity and the redox sensing of All4978.

Chemical Reduction and Spectroelectrochemical Titration—The chemical reduction was performed by adding a freshly prepared solution of sodium dithionite (Fig. 3). The effect of reduced FMN was investigated, too, because it has been reported to accelerate reduction of DosS (15). However, the presence or absence of FMN did not affect the kinetics of the reduction of $GAF_{All4978}$ with 1 mM $Na_2S_2O_4$. The reduction rate was not increased by the addition of ascorbic acid, GSH, FAD, or NADH (data not shown). Similar to reduction by sodium dithionite, the electrochemical titration led to a shift of the 427-nm Soret band and modification of the α-band at 559 nm (Fig. 4). Fits of the electrochemical titration curves yielded inflections at −449 mV (−445 ± 2 mV for the 424-nm band and −453 ± 2 mV for the 559-nm band) *versus* SHE. The mean, −449 mV *versus* SHE, is a remarkably low reduction potential for a heme protein (35).

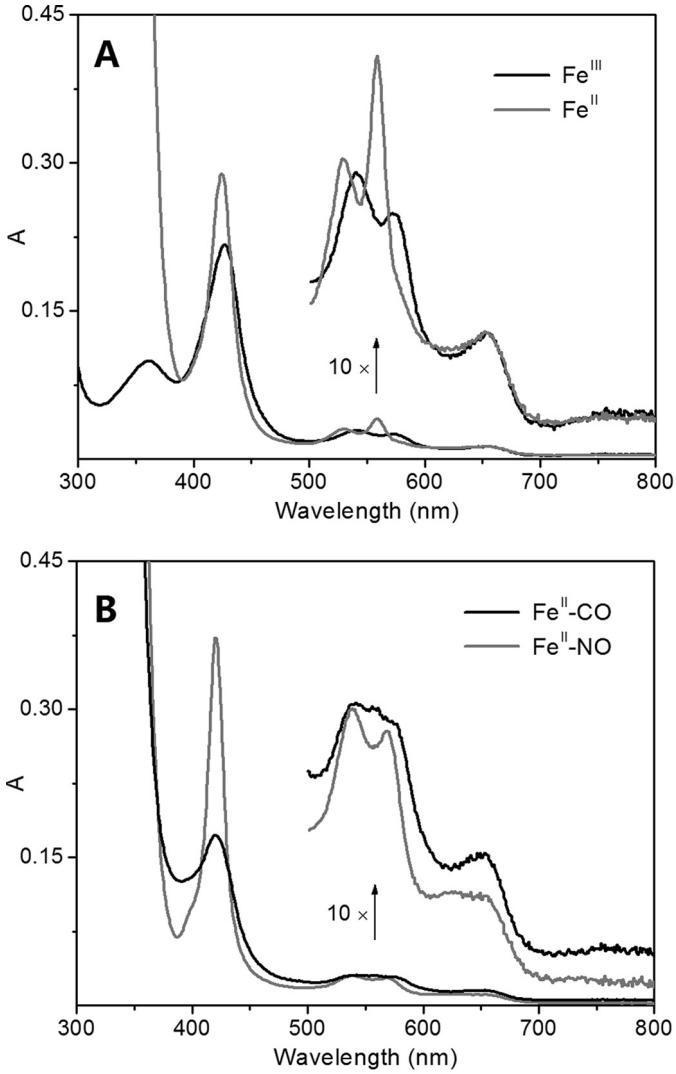

FIGURE 3. **Absorption spectra of different ligation states of $GAF_{All4978}$.** *A*, ferric form, as isolated (*black*), and ferrous form upon reduction (*gray*). *B*, CO-bound (*black*) and NO-bound (*gray*) upon reduction.

RR and MCD Spectroscopy Reveal Low Spin State and Hexacoordination of the Ferric $GAF_{All4978}$—RR spectra of frozen solutions were recorded with excitation into the blue edge of

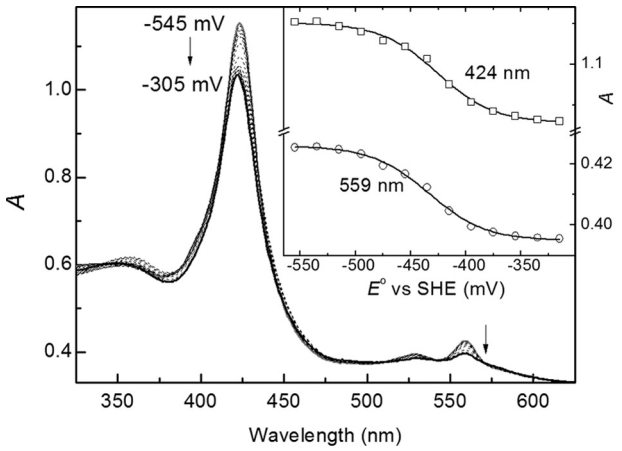

FIGURE 4. **Spectroelectrochemical titration of $GAF_{All4978}$, beginning at −545 mV.** Both the 424- and 559-nm bands reveal a remarkably low reduction potential E_0 of −445 ± 2 and −453 ± 2 mV, respectively.

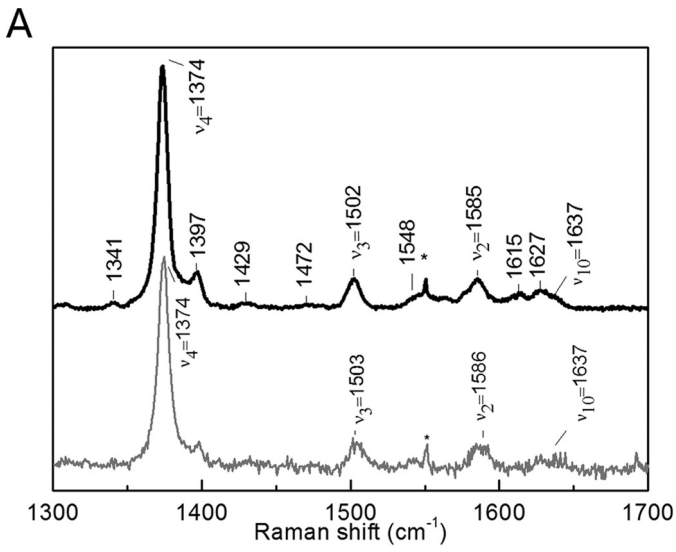

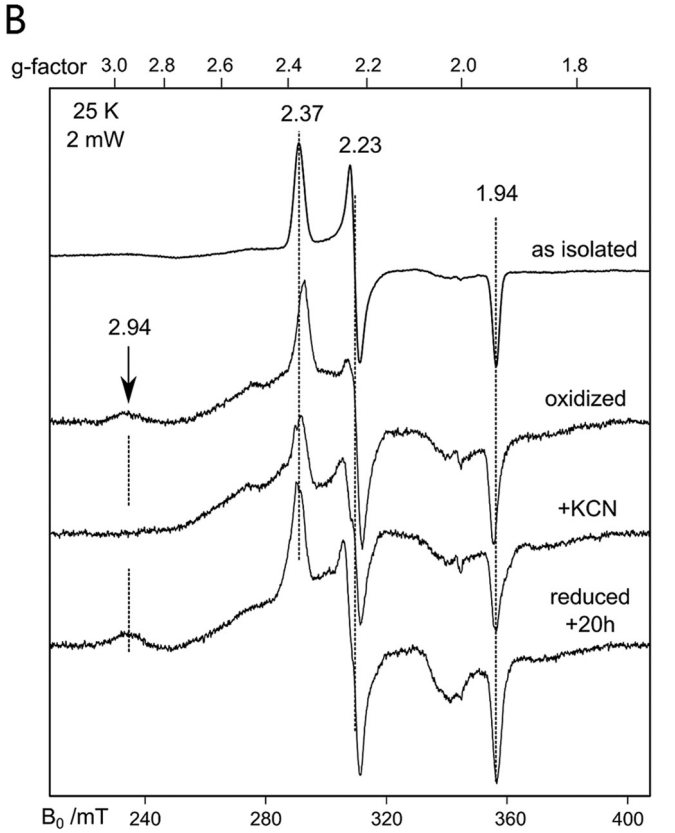

FIGURE 5. *A,* RR spectrum (high frequency region) of (*top*) ferric $GAF_{All4978}$ as isolated. *Bottom,* ferric $GAF_{All4978}$ after reduction and re-oxidation (20 mM KP_i at 77 K; λ_{ex} = 406.7 nm). *B,* EPR spectra of $GAF_{All4978}$ in as isolated (*top trace*), $K_6Fe(CN)_3$-oxidized form (*2nd trace*), cyanide-bound form (*3rd trace*), and reduced form exposed to air for 20 h (*bottom trace*).

the Soret band (406.7 nm). The RR spectrum of the as isolated $GAF_{All4978}$ recorded at 77 K is shown in Fig. 5, and the most relevant modes are summarized in Table 2. The observation of an intense so-called oxidation state marker transition, ν_4 appearing at 1374 cm^{-1} typical of ferriheme proteins (36, 37), provides further evidence that as isolated $GAF_{All4978}$ contains a ferriheme. Another important feature is the so-called spin-state marker transition, ν_3 appearing at 1502 cm^{-1}, which is a fingerprint for hexa-coordinated low-spin (6cLS) heme (1500–1510 cm^{-1}) (38). The positions of other prominent core marker bands (*e.g.* ν_2 and ν_{10}) are also consistent with a 6cLS heme (39). The $\nu_{C=C}$ modes characteristic of the heme vinyl substituents are well separated (1615 and 1627 cm^{-1}), indicating a rather different environment of the vinyl groups of rings A and B (36, 40).

MCD spectroscopy is another useful method for the exploration of iron coordination and spin-state in heme proteins (41–44). Room temperature spectra of the as isolated $GAF_{All4978}$ (Fig. 6) yielded characteristic signatures of ferric LS hemes that are less complex than those of the corresponding HS (S = 5/2) electron configuration (42). The ferriheme MCD spectrum of $GAF_{All4978}$ is similar to the LS spectrum of the His/Met-liganded cytochrome *c* (45), and Cys-liganded cytochrome P450s, the latter assignment being in line with the EPR results described above (46–49).

RR and MCD Spectroscopy Reveal Histidine Ligation of Ferrous $GAF_{All4978}$—RR spectra of the heme iron in the diamagnetic LS form, $GAF_{All4978}[Fe^{II}\text{-}CO]$ (S = 0), or in the paramagnetic HS form, HS $GAF_{All4978}[Fe^{II}]$ (S = 2), provide information on the modified coordination environment induced by cofactor reduction. Reduced samples without (5c) and with an extra ligand (NO or CO) (6c) at the Fe^{II} were measured under the same conditions, but in the absence of oxygen (Fig. 7 and Table 2). The most prominent core-size marker band of heme proteins in the high frequency region is the oxidation state marker ν_4 that indicates the presence of Fe^{III} (1370–1375 cm^{-1}) or Fe^{II} (1350–1375 cm^{-1}) (36, 37, 50–52). For the unliganded species, the ν_4 = 1359 cm^{-1} mode clearly demonstrates that the iron is in its reduced state. A shoulder at 1375 cm^{-1} may indicate the presence of a small fraction of ferric form. The above-mentioned spin-state marker ν_3 changes with the spin state of iron but is independent of the oxidation state, *i.e.* 1460–1470 cm^{-1} for 5cHS Fe^{II} and 1490–1510 cm^{-1} for 5cLS or 6cLS Fe^{II} (38, 51, 52). Therefore, the spectral features seen at 1493 and 1501 cm^{-1} indicate a LS complex for both sixth ligands, NO and CO. This is also consistent with the positions of ν_2 and ν_{10}.

Upon addition of the strong ligands NO and CO, the oxidation state marker band shifted to 1374 and 1372 cm^{-1}, respec-

TABLE 2

Core marker bands of $GAF_{All4978}$ in the ferric state as isolated and in the ferrous state without (5c) and with various distal ligands (6c)

Data from RR spectroscopy (λ_{ex} = 406.7 nm) at 77 K.

Mode	Ferric/cm^{-1}, as isolated	Ferrous/cm^{-1}		
		No ligand	NO	CO
ν_2	1585	1580	1578	1579
ν_3	1502	1493/1501	1503	1501
ν_4	1374	1359	1374	1372
ν_7		674	677	677
ν_{10}	1637	1619	1637	1629
ν_{15}		747	754	752

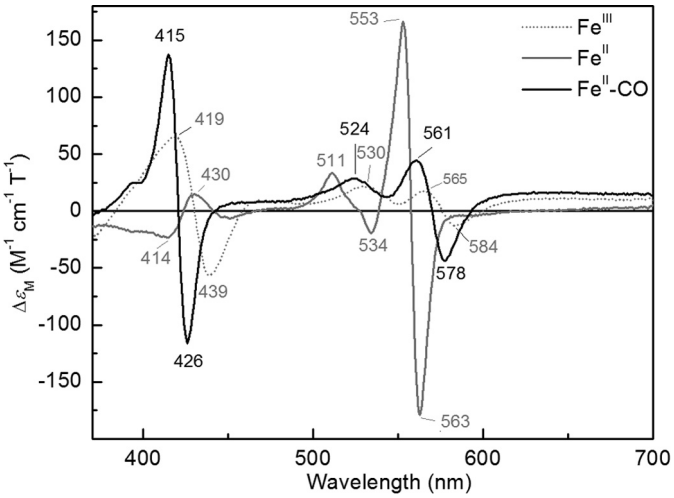

FIGURE 6. **MCD spectra of $GAF_{All4978}$ recorded at room temperature (B = 1.4 tesla) in 20 mM KP_i.** The spectrum of the as isolated form is given as a *dotted line*. The ferrous form (*gray*) was generated in a nitrogen atmosphere upon addition of 2 mM $Na_2S_2O_4$. The carbonyl liganded sample (*black*) was prepared in a CO atmosphere upon addition of 2 mM $Na_2S_2O_4$.

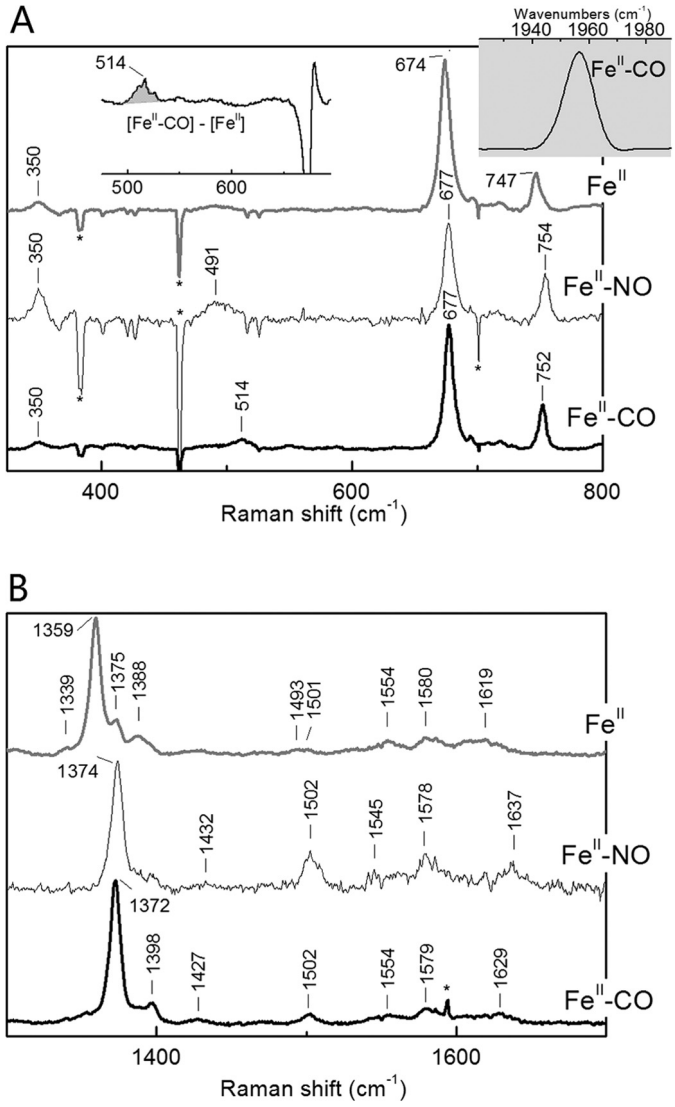

FIGURE 7. **RR spectroscopy (λ_{ex} = 406.7 nm) of frozen samples (77 K) of ferroheme $GAF_{All4978}$ in 20 mM KP_i without ligand (5c, *gray, in bold*) and with NO (*black, thin line*) and CO (*black, in bold*) as sixth ligand.** *A,* low frequency part. *Top,* difference spectrum (*black*) between $GAF_{All4978}$ [Fe^{II}] and $GAF_{All4978}$ [Fe^{II}-CO] is displayed to identify ν_{Fe-CO}. The resulting band at 514 cm^{-1} was fitted with a single Voigt function (*gray inset*). The *inset* shows the C=O band in the FTIR spectrum of the sample recorded at 25 °C. *B,* high frequency part.

tively, values typical of ferroheme nitrosyls and carbonyls (53). In contrast, the spectra are rather similar to each other and also to the unliganded sample that is consistent with the expected 6cLS situation. More importantly, the low frequency region of the Fe^{II}-CO spectrum can be used for the assignment of the ν_{Fe-CO} = 514 cm^{-1} stretch vibration by subtraction of the spectrum of the unliganded form. The anti-correlation of the C–O bond strength and the Fe–C bond strengths strongly depends on the ligand *trans* to the CO. This is a result of the σ competition between CO and the axial ligand for the d_z^2 acceptor orbital of iron. Thus, the pair of ν_{Fe-CO} and ν_{C-O} vibrational frequencies, the latter of which was obtained by FTIR spectroscopy (Fig. 7*A, inset*), can be used to assign the proximal ligand type. In Fig. 8, the position of $\nu_{Fe-CO}|\nu_{C-O}$ falls within the anti-correlations of thiolate-liganded hemes, His-liganded heme proteins, and 5c-liganded hemes. Clearly, Cys is not the proximal ligand. However, $GAF_{All4978}$[Fe^{II}–CO] lies surprisingly close to the 5c line. A similar position was found for the case of $\nu_{Fe-CO}|\nu_{C-O}$ of Rev-erbβ (54), which is His-liganded in the CO-bound form. To complete the Raman measurements, the ferrous-state sample was exposed to air, yielding (see above) again the ferric state protein (λ_{max} = 413 nm), again showing the same Raman spectrum as measured for the as isolated form of $GAF_{All4978}$.

The MCD and the absorbance spectrum of the reduced/CO-bound system further supports a His-liganded type of CO heme. A number of other redox-dependent ligand-switch proteins, *e.g.* CooA, Rev-erbβ, and *Drosophila* E75, show similar MCD peak positions (supplemental table in Ref. 54). We therefore conclude that in the reduced state the CO-coordinated heme is ligated by a histidine residue instead of the cysteine found in the oxidized state.

A ligand switch between a cysteine and a histidine residue, which is dependent on the oxidation state of the iron atom of heme, has been reported for a number of heme-binding proteins (Table 3) (54–60). All4978 displays an interesting sequence motif (^{95}HDHGH) in the region below the heme ring plane; any one of these three histidines might represent the putative switching partner. A close-by cysteine residue (Cys-92) might be the other ligand-switching partner. Accordingly, a number of variant proteins were prepared by site-directed mutation, and their heme binding capability was determined.

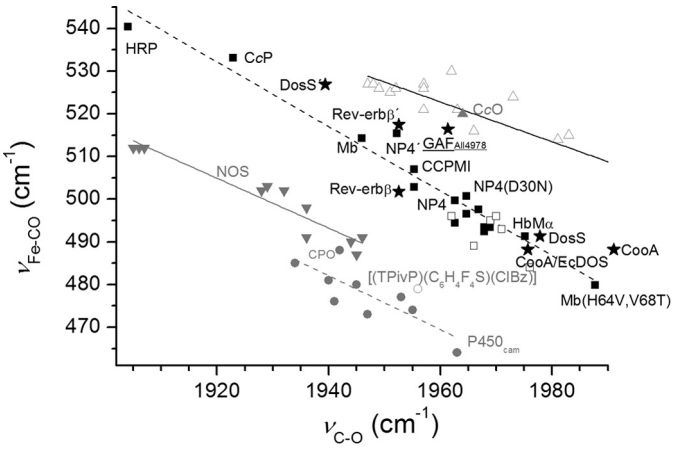

FIGURE 8. **Anticorrelation plot of $\nu_{C\text{-}O}$ *versus* $\nu_{Fe\text{-}CO}$.** It was previously demonstrated (53) that the CO complexes of ferrohemes fall into four groups as follows: (i) Cys-coordinated cytochrome P450 type (*gray dashed line*); (ii) the Cys-coordinated nitric-oxide synthases type (*NOS, gray solid line*) (70, 71); (iii) His-coordinated protein heme and imidazole-synthetic heme models (*black dashed line*) (72); and (iv) 5-coordinate hemes (*black solid line*, mainly model compounds) (73). Proteins are displayed as *filled symbols* and model compounds as *open symbols*. The heme sensor proteins DosS (69), Rev-erbβ (54), CooA (67, 74), *Ec*DOS (75), and $GAF_{All4978}$ (this work) are displayed as *stars*. The abbreviations used are as follows: *CcP*, cytochrome *c* peroxidase; *ClBz*, chlorobenzene; *CooA*, CO-sensing transcription factor from *Rhodospirillum rubrum*; *CPO*, chloroperoxidase; *DosS*, GAF A domain of the histidine kinase DosS from *M. tuberculosis*; *EcDOS*, heme-regulated phosphodiesterase from *E. coli*; *HbM*α, hemoglobin M Boston-α; *HRP*, horseradish peroxidase; *P450*, cytochrome $P450_{cam}$; *Rev-erb*β, human transcription factor; *TpivP*, picket fence porphyrin.

The suggested function of Cys-92 could be verified from C92S/C92G variants; both mutations led to nearly complete loss of heme incorporation (C92S showed ~10% heme content compared with the heme content of the WT protein, and C92G ~6%, respectively, see Table 1 (keep in mind that the heme loading of the WT protein itself is relatively low)). However, the assignment which of the three candidate histidine residues is serving as ligand in the Fe^{II} state is not straightforward. Single mutations of all three histidine residues led to a decrease in heme binding. For His-95 variants (H95A/H95G), binding was reduced to 46 and 37%, respectively. For both His-97 and His-99 variants, a more dramatic decrease was observed (Table 1) as follows: H97A/H97G contained 12 and 9%, respectively, and H99A carried only 10% of the WT heme content. This result seems to support assigning the axial ligand switch to either His-97 or His-99. Moreover, mutating one of the interspersed non-histidine residues reduces the heme content to the same extent; D96A lost nearly 80% of the WT heme content (residual amount of ~18%, see Table 1), and thus all three His residues remain viable. It is noted however that sequence alignment with GAF_{DosS} (see below) supports assigning His-95 as the axial ligand switch (Fig. 1). Moreover, as GAF_{DosS} does not undergo a Cys → His switch and thus does not carry a cysteine at the corresponding position, reliance of the sequence alignment alone is somewhat uncertain.

Homology Modeling—Heme binding GAF domains are found in two histidine kinases, DosS and DosT, from *M. tuberculosis*. Both GAF_{DosS} and GAF_{DosT} have been structurally characterized by x-ray crystallography (PDB code 2W3G (15) and 2VZW (10), respectively). Sequence alignments between $GAF_{All4978}$ and GAF_{DosS} or GAF_{DosT} using T-Coffee (Fig. 1) (14) revealed high amino acid sequence homologies (69 and 68%, respectively). In addition, secondary structure predictions of $GAF_{All4978}$ using PSIPRED closely matched secondary structural elements of GAF_{DosS} and GAF_{DosT} (61). Homology models built with PDB code 2W3G as template resulted in higher quality parameters than models built with PDB code 2VZW. The former model based on the structure of GAF_{DosS} (Fig. 9*A*) was investigated in more detail. To allow docking in the pocket, the heme had to be rotated by ~180° around the *z* axis, which passes through the iron and is perpendicular to the heme plane. After this rotation, the protein structures of GAF_{DosS} and $GAF_{All4978}$ show a high degree of homology (root mean square deviation value of 0.57 Å for the backbone atoms calculated by Swiss-PdbViewer (27, 28)).

The ^{92}C*XX*HDHGH motif lies in a loop region. In GAF_{DosS}, His-149 had been identified as the proximal ligand to the heme group, and it is located in a loop region connecting the β3- and β4-strands (Pro-140 to Thr-154) (15). The sequence alignments (Fig. 1*A*) reveal that His-95 of $GAF_{All4978}$ corresponds to His-149 of GAF_{DosS}. Thus, in the $GAF_{All4978}$ model, His-95 was inserted as the heme ligand of the iron in the reduced (Fe^{II}) state, as identified by the spectroscopic results discussed above. In addition, to accommodate the requirement that the iron in the oxidized (Fe^{III}) state has a Cys coordination, the sequence alignment was modified by placing Cys-92 of $GAF_{All4978}$ in line with His-149 of GAF_{DosS}, and the model building was repeated. The His-95- and the Cys-92-liganded forms are compared with each other in Fig. 9*B*, showing the two peptide chains in *blue* and *yellow*, respectively. Both proximal ligands are located in a highly flexible region of the structure that may support ligand switching. The model indicates that the conformational change may create a large rearrangement in the turn Ile-82–Gly-98, but nevertheless it preserves the overall structure of $GAF_{All4978}$.

DNA Binding—The presence of the C-terminally located HtH motif called for attempts identifying DNA binding capacity of All4978. A survey in the genome neighborhood did not yield any apparent interacting gene product or an operon structure. All4978 is followed by two genes encoding ribosomal RNA (16S and 23S) and is preceded by a gene encoding for a hypothetical protein. A gene for a hypothetical protein is also found on the opposite strand. Thus, due to the absence of genes that might potentially be functionally related and be regulated by All4978, we suggested autoregulation by binding to its own promotor. Similar experiments had been reported for other switchable DNA-binding proteins, *e.g.* EL222 from *Erythrobacter litoralis* (62). This protein serves as a blue light sensor that (preferentially in its lit state) binds to a short stretch of its own promotor. In fact, control experiments using EL222 (courtesy Dr. Kevin Gardner, City University of New York) as reference and even a hybrid protein composed of the heme-binding GAF domain of All4978 and the DNA-binding HtH domain of El222 showed the expected binding to the EL222 target DNA (data not shown). Under the same conditions established for the control experiments, we performed binding studies with All4978, using a 25-bp stretch of DNA as target. Applying increasing amounts of All4978, we find clear evidence for a protein-DNA complex. Under the experimental conditions,

TABLE 3

Selected examples of ligand switching sensory heme proteins with ferric Fe-S_{Cys} and ferrous Fe-N_{His} coordination

The following abbreviations are used: CRP, cAMP receptor protein; eIFα, eukaryotic initiation factor 2α; HRI, heme-regulated eIFα kinase; P450, cytochrome P450; PpsR, heme-binding and DNA-binding transcription factor of *R. sphaeroides*.

Protein	Organism	Domain fold	Motif	Function
$GAF_{All4978}$	*Nostoc* sp. PCC7120	GAF	CPRHDHGH	DNA binding
CooA (55)	*R. rubrum*	CRP	CMH	CO sensing, DNA binding
Rev-erbβ (54, 56)	Vertebrates	Nuclear receptor	HLVCP	Nuclear receptor
E75 (54, 57)	Invertebrates	Nuclear receptor	$CPX_{18}H/HX_{31}CP$	Transcription factor
HRI (58)	Mammals		CP	Kinase of eIFα
NPAS2 (59)	Mammals	PAS	CH	Transcriptional regulator
PpsR (60)	*R. sphaeroides*	HtH/PAS	$HX_{148}CI$	DNA binding

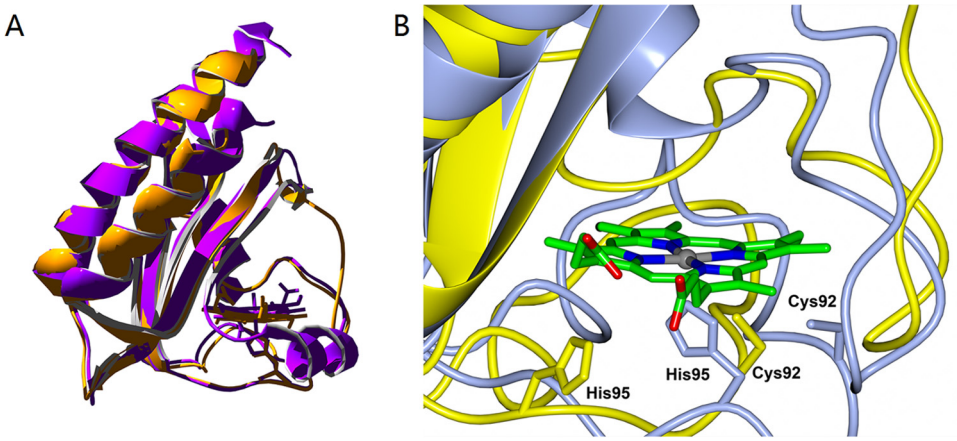

FIGURE 9. *A,* comparison of the homology model of $GAF_{All4978}$(17–149) with His-95 as proximal heme ligand (*orange*) and with the x-ray structure of GAF_{DosS} (PDB code 2W3G) (15) (*purple*). *B,* comparison of the heme pocket of the homology model of $GAF_{All4978}$ with His-95 (*blue ribbons*) or Cys-92 (*yellow*) as proximal heme ligand. Figures were prepared with Swiss-PdbViewer 4.1(28) and rendered with POV-Ray 3.6.

only the ferric form of the protein generated a DNA-protein complex formation (Fig. 10). One should mention that maintaining reducing conditions through the entire experiment is not easy, so any trace of a protein-DNA complex formed might be due to partial re-oxidation. If only the GAF domain of All4978 was used in these experiments, no complex formation was observed (data not shown).

Discussion

$GAF_{All4978}$ represents a new heme-binding GAF domain protein; there are only few examples reported so far (9, 11), and none have yet been identified in cyanobacteria. As part of the genome-annotated transcription regulator All4978, it carries an HtH motif at its C-terminal end as a signaling motif, making these proteins from *Nostoc* the first showing such domain composition. Although $GAF_{All4978}$ shares a high degree of structural homology with GAF_{DosS} and GAF_{DosT}, the heme iron coordination is entirely different with a Cys sulfur acting as the axial ligand of the iron in its ferric oxidation state. Like GAF_{DosS}, but unlike GAF_{DosT} (5), the protein is not able to bind O_2 despite its facile oxidation within seconds. A similar experiment, as reported previously (5), gave additional proof that $GAF_{All4978}$ does not bind oxygen; addition of cyanide to the oxidized form yields an absorbance peak at 540 nm as reported for GAF_{DosS} (Fig. 5*B*). However, in contrast to GAF_{DosS}, reduction of the heme cofactor of $GAF_{All4978}$ by $S_2O_4^{2-}$ was not enhanced in the presence of cytosolic reducers like FMN ($E^\circ = -220$ mV) and NAD^+ ($E^\circ = -320$ mV) (63), suggesting its heme cofactor has a very low reduction potential as compared with typical heme irons. Although no intracellular potential has been reported for *Nostoc,* one might assume a redox sensing by the proteins described here. *Nostoc* forms heterocysts capable of nitrogen fixation, only under very reducing conditions allowing nitrogenase activity. When the intracellular potential is increased, *Nostoc* cells stop nitrogen fixation, potentially concurrent with changing into the ferric state of the heme-binding proteins. Such conversion needs to be rapid in order to protect the oxygen-sensitive nitrogenase complex. The ineffectiveness of naturally occurring mediators was corroborated by the spectroelectrochemical titration measurements that yielded a midpoint potential for the hemes of -445 ± 2 and -453 ± 2 mV, respectively (Soret and α-band monitored). Interestingly, reduction with $S_2O_4^{2-}$ ($E^\circ = -660$ mV) (64) causes a ligand switch from Cys-92 to His-95. Such behavior representing an activation/de-activation switch is well established for a number of other heme sensory proteins with very distinct folds (Table 3) (3, 59, 65).

The high degree of structural homology between $GAF_{All4978}$ and GAF_{DosS} allowed building a structural model of $GAF_{All4978}$ for both its oxidized (Cys-92 liganded) and reduced (His-95 liganded) forms (Fig. 9). Verification of His-95 as the proximal ligand in the ferrous state remains uncertain to some extent; the sequence alignment gives preference to His-95, whereas the mutagenesis experiments would be more consistent with either His-97 or His-99. Ligand switching has also been reported for other heme-binding proteins where it was identified as activation/de-activation mechanism for sensor functions (Table 3). A similar mechanism might be envisaged here for $GAF_{All4978}$, which carries an HtH motif in its C-terminal domain.

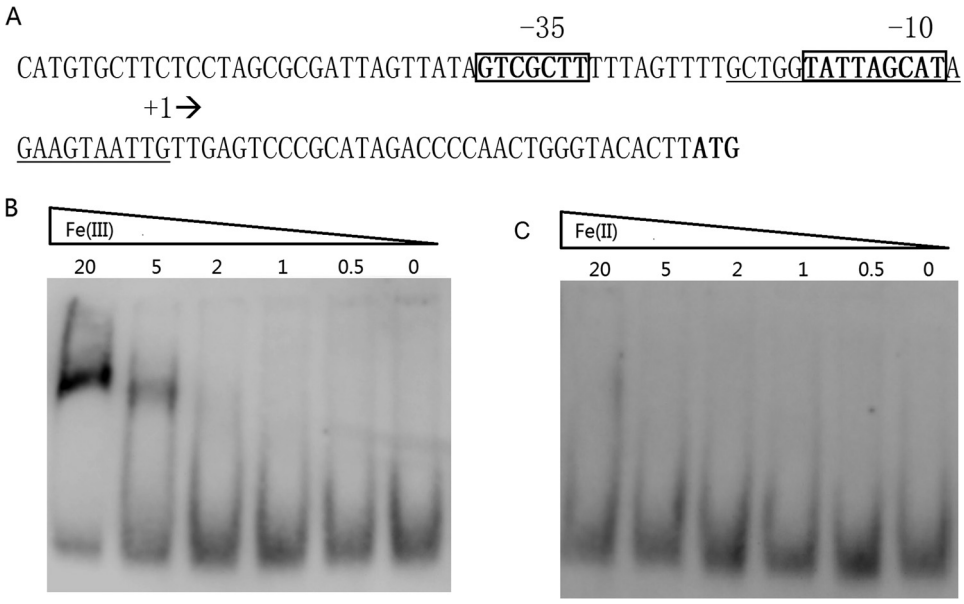

FIGURE 10. **EMSA of All4978 with promoter DNA.** *A*, the upstream sequence of All4978 was analyzed by the BPROM program. The putative −10 and −35 regions of the promoter are shown in *bold* and *boxed*. The position of the transcriptional start site is indicated by an *arrow*. The start codon (ATG) of All4978 is shown in *bold*. The nucleotide sequence *underlined* was synthesized for the binding assay. *B*, EMSA of All4978 in ferric state. *C*, EMSA of All4978 in ferrous state. Protein concentrations were 20, 5, 2, 1, 0.5, and 0 μM. Concentration of digoxigenin-labeled DNA in all experiments was 15 nM.

Changing the coordinating ligand upon reduction is understood as a consequence of the loss of charge stabilization between $CysS^-$ and the heme iron as shown in Reaction 1,

$$(ppIX)Fe^{+}\text{–}{}^{-}S_{Cys} + e^{-} + N_{His} + H^{+} \rightarrow (ppIX)Fe\text{–}N_{His} + HS_{Cys}$$

REACTION 1

One might assume that the conformational change induced by the ligand switch results in modulation of a catalytic or DNA binding domain associated with the sensory heme domain. An example for this process is found for CooA, a transcriptional activator. Here, a Cys-His switch was accomplished by CO binding, which then allows formation of the DNA complex. The ligand switch was examined by NMR and EPR spectroscopy (66).

Examples of other ligand-switching heme proteins are presented in Table 3. Supported by the mutagenesis experiments (Table 1), other Cys, His, and Met residues in the $GAF_{All4978}$ structure can be excluded as heme ligands. Among the folds for which sensory heme domains were found, PAS domains may be mentioned because they share a high degree of structural homology with GAF domains. A structural feature among many, but not all, heme sensory proteins is the presence of a Pro following the coordinating Cys (67). This CP motif is also present in $GAF_{All4978}$ (Table 3 and Fig. 1). Another common feature of ligand-switching heme sensors is that the coordinating His residue is mostly found at the positions of aa 1–3 away from the CP motif, but there are exceptions where the distance in sequence can be much larger (Table 3). An example is the nuclear receptor E75 (54, 57), where a relatively large distance between the CP motif and the putative His ligand is proposed.

A special case has been reported for the HtH transcription factor PpsR (a heme-binding and DNA-binding transcription factor) expressed in the photosynthetic bacterium *Rhodobacter sphaeroides*, which contains two PAS domains (60). In this case, the heme-binding Cys is located in the HtH domain, whereas the ligand-switching His residue (upon reduction) was identified as part of one of the PAS domains, suggesting that the heme binding pocket is formed as part of an interdomain surface. Here, the heme-coordinating Cys is followed by an Ile residue. In summary, the currently known ligand-switching heme sensory domains show very large fold diversity. $GAF_{All4978}$ and its paralogs in *Nostoc* extend this diversity and represent the first example of a ligand-switching heme-GAF domain. Apparently, the sensing mechanism among heme-binding GAF domains is accomplished in many different ways.

An important structural and functional aspect among the heme-sensing proteins is the nature of the proximal ligand, which also shows a very high degree of diversity involving water, Glu, His, and N-terminally Pro (68). The spectroscopic analysis for $GAF_{All4978}$ clearly demonstrates a 6cLS complex in case of the ferric form. However, the structural models do not provide evidence for a 6th side-chain ligand. In the case of GAF_{DosS} and GAF_{DosT}, a proximal Tyr plays a critical role for the sensory function (10, 15, 69). Similar as in these two proteins, Tyr-41 of $GAF_{All4978}$ is located in the model above the heme ring plane, yet at a relatively large distance to the iron (4.3 Å), making a bond formation between the iron and the phenolic oxygen fairly unlikely. In fact, the finding of similar results for the wild-type protein and its Y41F/Y41G mutants speaks against a direct involvement of Tyr-41 unlikely. Alternatively, a water molecule might be positioned in between serving as a ligand that is replaced by NO or CO in the reduced state. There exists no other protein residue candidate for this ligand. In contrast, P450s also exhibit 6cLS spectra in case of the substrate-unbound state, suggesting that the ligand field of Cys^- together with a proximal water ligand is strong enough to create the LS

state.[7] Surprisingly, even diatomic ligands with high affinity for ferric hemes, *i.e.* NO or CN^-, did not bind to the ferric (Fe^{III}) form of $GAF_{All4978}$, suggesting that the distal pocket must be rather crowded. Such crowding could be explained by the presence of the Tyr-41 side chain reaching into the distal pocket.

Further information on the function of All4978 might be obtained by studying this protein in its genuine host. In particular, the extent of heme loading, the identification of the sixth ligand, and potentially also the redox switch-dependent regulation of gene expression might be determined. Such work, however, requires a different approach that is currently beyond the scope of this work.

Judged from the homology models and in agreement with literature reports of other heme sensory domains (Fig. 9*A*) (68), ligand switching induces large conformational changes, which also is demonstrated by the ability of the Fe^{II} form to bind CO and NO. However, as indicated above, the low reduction potential calls for a proof-of-function as redox sensor under physiological conditions. It is known that photosynthetic organisms show rather low potentials. Sensors may be adapted in this scenario to shutting down electron transport in case the acceptor is saturated.

Another possible function would be sensing of a ferriheme ligand. As strong diatomic ferriheme ligands do not bind to the distal heme site, it is difficult to imagine what this ligand may be. A possible explanation might be that protein-DNA interaction(s) accomplished via the HtH motif introduce conformational changes, thus allowing either the reduction potential to rise and/or (a) ligand(s) to bind and to activate signal transduction.

The protein was found as a dimer, irrespective of its state of oxidation. This raises the question for the mechanism of DNA binding, as usually HtH motifs bind as dimers, which under the constitutively dimeric composition determined here would make a regulation difficult to understand. However, one might consider the yet speculative oxidation state-dependent formation of a heterodimeric complex with another transcription factor in the presence of the DNA target.

Preliminary results point to binding to a sequence isolated from the promotor region of All4978, preferentially when the protein is in the ferric state. Further investigations on the precise binding site and the binding mechanism, *e.g.* homodimer to heterodimer change (see above), will require experiments extending the results reported here.

Overall, this study adds a new type of heme pocket to the very diverse members of heme sensory domains. $GAF_{All4978}$ and possibly GAF_{7016} represent the first example of a combination of a GAF domain fold with a ligand-switching heme that has been reported for other folds found in Rev-erbβ and CooA. In addition, the full-length protein shows for the first time a combination of a heme-binding GAF domain with an HtH motif, which are typical motifs involved in gene expression regulation.

[7] It should be mentioned at this point that in the case of the heme-GAF domain of MA4561, imidazole was artificially bound to the distal heme site from IMAC protein purification (11). Because IMAC purification was used for the isolation of $GAF_{All4978}$ with imidazole elution as well, the protein was also eluted with EDTA for comparison. As a result, no spectroscopic differences were observed, demonstrating that imidazole did not bind to the heme pocket of $GAF_{All4978}$.

Author Contributions—K. -H. Z., W. G., K. T., and M. K. designed the study. K. T. purified proteins, conducted mutagenesis, and performed the DNA binding experiment. M. K. performed and analyzed the RR, FTIR, and electrochemical titrations. N. C. performed and analyzed the EPR. B. B. L. constructed the vectors for expression of the wild-type proteins. Q. H., R. S., and M. Z. contributed to the protein preparations. H. S., K. -H. Z., and W. G. wrote the manuscript.

Acknowledgments—We thank Marian Stapper and Norbert Dickmann for technical assistance. We also thank Dr. Olaf Rüdiger (Max Planck Institute for Chemical Energy Conversion) for valuable discussion and Prof. W. Lubitz (Max Planck Institute for Chemical Energy Conversion) for generous support. We thank Dr. Kevin Gardner (City University of New York) and Dr. Laura Motta-Mena (University of Texas Southwestern Medical Center) for generously providing the plasmid encoding EL222. We are grateful to Dr. Karin Meierhoff (University of Düsseldorf) for support for the DNA binding assay.

References

1. Gilles-Gonzalez, M. A., and Gonzalez, G. (2005) Heme-based sensors: defining characteristics, recent developments, and regulatory hypotheses. *J. Inorg. Biochem.* **99,** 1–22
2. Sun, Y., Zeng, W., Benabbas, A., Ye, X., Denisov, I., Sligar, S. G., Du, J., Dawson, J. H., and Champion, P. M. (2013) Investigations of heme ligation and ligand switching in cytochromes P450 and P420. *Biochemistry* **52,** 5941–5951
3. Girvan, H. M., and Munro, A. W. (2013) Heme sensor proteins. *J. Biol. Chem.* **288,** 13194–13203
4. Dawson, J. H., and Sono, M. (1987) Cytochrome P-450 and chloroperoxidase: thiolate-ligated heme enzymes. Spectroscopic determination of their active site structures and mechanistic implications of thiolate ligation. *Chem. Rev.* **87,** 1255–1276
5. Kumar, A., Toledo, J. C., Patel, R. P., Lancaster, J. R., Jr., and Steyn, A. J. (2007) *Mycobacterium tuberculosis* DosS is a redox sensor and DosT is a hypoxia sensor. *Proc. Natl. Acad. Sci. U.S.A.* **104,** 11568–11573
6. Green, J., Crack, J. C., Thomson, A. J., and LeBrun, N. E. (2009) Bacterial sensors of oxygen. *Curr. Opin. Microbiol.* **12,** 145–151
7. Knipp, M., and He, C. (2011) Nitrophorins: Nitrite disproportionation reaction and other novel functionalities of insect heme-based nitric oxide transport proteins. *IUBMB Life* **63,** 304–312
8. Ho, Y. S., Burden, L. M., and Hurley, J. H. (2000) Structure of the GAF domain, a ubiquitous signaling motif and a new class of cyclic GMP receptor. *EMBO J.* **19,** 5288–5299
9. Sardiwal, S., Kendall, S. L., Movahedzadeh, F., Rison, S. C., Stoker, N. G., and Djordjevic, S. (2005) A GAF domain in the hypoxia/NO-inducible *Mycobacterium tuberculosis* DosS protein binds haem. *J. Mol. Biol.* **353,** 929–936
10. Podust, L. M., Ioanoviciu, A., and Ortiz de Montellano, P. R. (2008) 2.3 Å x-ray structure of the heme-bound GAF domain of sensory histidine kinase DosT of *Mycobacterium tuberculosis*. *Biochemistry* **47,** 12523–12531
11. Molitor, B., Stassen, M., Modi, A., El-Mashtoly, S. F., Laurich, C., Lubitz, W., Dawson, J. H., Rother, M., and Frankenberg-Dinkel, N. (2013) A heme-based redox sensor in the methanogenic archaeon *Methanosarcina acetivorans*. *J. Biol. Chem.* **288,** 18458–18472
12. Ioanoviciu, A., Yukl, E. T., Moënne-Loccoz, P., and de Montellano, P. R. (2007) DevS, a heme-containing two-component oxygen sensor of *Mycobacterium tuberculosis*. *Biochemistry* **46,** 4250–4260
13. Sousa, E. H., Tuckerman, J. R., Gonzalez, G., and Gilles-Gonzalez, M. A. (2007) DosT and DevS are oxygen-switched kinases in *Mycobacterium tuberculosis*. *Protein Sci.* **16,** 1708–1719
14. Notredame, C., Higgins, D. G., and Heringa, J. (2000) T-Coffee: A novel method for fast and accurate multiple sequence alignment. *J. Mol. Biol.*

302, 205–217
15. Cho, H. Y., Cho, H. J., Kim, Y. M., Oh, J. I., and Kang, B. S. (2009) Structural insight into the heme-based redox sensing by DosS from *Mycobacterium tuberculosis*. *J. Biol. Chem.* **284,** 13057–13067
16. Ohmori, M., Ikeuchi, M., Sato, N., Wolk, P., Kaneko, T., Ogawa, T., Kanehisa, M., Goto, S., Kawashima, S., Okamoto, S., Yoshimura, H., Katoh, H., Fujisawa, T., Ehira, S., Kamei, A., *et al.* (2001) Characterization of genes encoding multi-domain proteins in the genome of the filamentous nitrogen-fixing Cyanobacterium *Anabaena* sp. strain PCC 7120. *DNA Res.* **8,** 271–284
17. Rockwell, N. C., and Lagarias, J. C. (2010) A brief history of phytochromes. *ChemPhysChem* **11,** 1172–1180
18. Maris, A. E., Sawaya, M. R., Kaczor-Grzeskowiak, M., Jarvis, M. R., Bearson, S. M., Kopka, M. L., Schröder, I., Gunsalus, R. P., and Dickerson, R. E. (2002) Dimerization allows DNA target site recognition by the NarL response regulator. *Nat. Struct. Biol.* **9,** 771–778
19. Tang, K., Zeng, X. L., Yang, Y., Wang, Z. B., Wu, X. J., Zhou, M., Noy, D., Scheer, H., and Zhao, K. H. (2012) A minimal phycobilisome: fusion and chromophorylation of the truncated core-membrane linker and phycocyanin. *Biochim. Biophys. Acta* **1817,** 1030–1036
20. Teale, F. W. (1959) Cleavage of the haem-protein link by acid methylethyl ketone. *Biochim. Biophys. Acta* **35,** 543
21. Berry, E. A., and Trumpower, B. L. (1987) Simultaneous determination of hemes *a*, *b*, and *c* from pyridine hemochrome spectra. *Anal. Biochem.* **161,** 1–15
22. Andersen, J. F., Ding, X. D., Balfour, C., Shokhireva, T. K., Champagne, D. E., Walker, F. A., and Montfort, W. R. (2000) Kinetics and equilibria in ligand binding by nitrophorins 1–4: evidence for stabilization of a nitric oxide-ferriheme complex through a ligand-induced conformational trap. *Biochemistry* **39,** 10118–10131
23. Ding, X. D., Weichsel, A., Andersen, J. F., Shokhireva, T. K., Balfour, C., Pierik, A. J., Averill, B. A., Montfort, W. R., and Walker, F. A. (1999) Nitric oxide binding to the ferri- and ferroheme states of nitrophorin 1, a reversible NO-binding heme protein from the saliva of the blood-sucking insect, *Rhodnius prolixus*. *J. Am. Chem. Soc.* **121,** 128–138
24. Stoll, S., and Schweiger, A. (2006) EasySpin, a comprehensive software package for spectral simulation and analysis in EPR. *J. Magn. Reson.* **178,** 42–55
25. Arnold, K., Bordoli, L., Kopp, J., and Schwede, T. (2006) The SWISS-MODEL Workspace: a web-based environment for protein structure homology modelling. *Bioinformatics* **22,** 195–201
26. Kiefer, F., Arnold, K., Künzli, M., Bordoli, L., and Schwede, T. (2009) The SWISS-MODEL repository and associated resources. *Nucleic Acids Res.* **37,** D387–D392
27. Guex, N., Peitsch, M. C., and Schwede, T. (2009) SWISS-MODEL and Swiss PdbViewer: automated comparative protein structure modeling with SWISS-MODEL and Swiss-PdbViewer: a historical perspective. *Electrophoresis* **30,** S162-S173
28. Guex, N., and Peitsch, M. C. (1997) SWISS-MODEL and the Swiss-PdbViewer: an environment for comparative protein modeling. *Electrophoresis* **18,** 2714–2723
29. van Gunsteren, W. F., Billeter, S. R., Eising, A. A., Hünenberger, P. H., Krüger, P., Mark, A. E., Scott, W. R., and Tironi, I. G. (1996) *Biomolecular Simulation: The GROMOS96 Manual and User Guide*, Vdf Hochschulverlag AG an der ETH Zürich, Zürich
30. Hooft, R. W., Vriend, G., Sander, C., and Abola, E. E. (1996) Errors in protein structures. *Nature* **381,** 272
31. Laskowski, R. A., MacArthur, M. W., Moss, D., and Thornton, J. M. (1993) PROCHECK: A program to check the stereochemical quality of protein structures. *J. Appl. Cryst.* **26,** 283–291
32. Smith, A. T., Marvin, K. A., Freeman, K. M., Kerby, R. L., Roberts, G. P., and Burstyn, J. N. (2012) Identification of Cys94 as the distal ligand to the Fe(III) heme in the transcriptional regulator RcoM-2 from *Burkholderia xenovorans*. *J. Biol. Inorg. Chem.* **17,** 1071–1082
33. He, C., Nishikawa, K., Erdem, Ö. F., Reijerse, E., Ogata, H., Lubitz, W., and Knipp, M. (2013) Complexes of ferriheme nitrophorin 4 with low-molecular weight thiol(ate)s occurring in blood plasma. *J. Inorg. Biochem.* **122,** 38–48
34. Taylor, C. P. (1977) EPR of low-spin heme complexes–relation of T2g hole model to directional properties of G-tensor, and a new method for calculating ligand-field parameters. *Biochim. Biophys. Acta* **491,** 137–148
35. Zheng, Z., and Gunner, M. R. (2009) Analysis of the electrochemistry of hemes with E(m)s spanning 800 mV. *Proteins* **75,** 719–734
36. Maes, E. M., Walker, F. A., Montfort, W. R., and Czernuszewicz, R. S. (2001) Resonance Raman spectroscopic study of nitrophorin 1, a nitric oxide-binding heme protein from *Rhodnius prolixus*, and its nitrosyl and cyano adducts. *J. Am. Chem. Soc.* **123,** 1164–1172
37. Kincaid, J. R. (2000) in *The Porphyrin Handbook* (Kadish, K. M., Smith, K. M., and Guilard, R., eds) pp. 225–291, 1st Ed., Academic Press, San Diego
38. Spiro, T. G., Stong, J. D., and Stein, P. (1979) Porphyrin core expansion and doming in heme proteins. New evidence from resonance Raman spectra of six-coordinate high-spin iron(III) hemes. *J. Am. Chem. Soc.* **101,** 2648–2655
39. Feis, A., Marzocchi, M. P., Paoli, M., and Smulevich, G. (1994) Spin state and axial ligand bonding in the hydroxide complexes of metmyoglobin, methemoglobin, and horseradish peroxidase at room and low temperatures. *Biochemistry* **33,** 4577–4583
40. Choi, S., Spiro, T. G., Langry, K. C., Smith, K. M., Budd, D. L., and La Mar, G. N. (1982) Structural correlations and vinyl influences in resonance Raman spectra of protoheme complexes and proteins. *J. Am. Chem. Soc.* **104,** 4345–4351
41. Sutherland, J. C., and Holmquist, B. (1980) Magnetic circular dichroism of biological molecules. *Annu. Rev. Biophys. Bioeng.* **9,** 293–326
42. Cheesman, M. R., Greenwood, C., and Thomson, A. J. (1991) Magnetic circular dichroism of hemoproteins. *Adv. Inorg. Chem.* **36,** 201–255
43. Dawson, J. H., and Dooley, D. M. (1989) in *Iron Porphyrins, Part 3* (Lever, A. B., and Gray, H. B., eds) pp. 1–93, VCH Publishers, Inc., New York
44. Cheek, J., and Dawson, J. H. (2000) in *The Porphyrin Handbook* (Kadish, K. M., Smith, K. M., and Guilard, R., eds) pp. 339–369, Academic Press, San Diego
45. Eaton, W. A., and Hochstrasser, R. M. (1967) Electronic spectrum of single crystals of ferricytochrome-*c*. *J. Chem. Phys.* **46,** 2533–2539
46. Sono, M., Andersson, L. A., and Dawson, J. H. (1982) Sulfur donor ligand binding to ferric cytochrome P-450-CAM and myoglobin. Ultraviolet-visible absorption, magnetic circular dichroism, and electron paramagnetic resonance spectroscopic investigation of the complexes. *J. Biol. Chem.* **257,** 8308–8320
47. Dawson, J. H., Trudell, J. R., Linder, R. E., Barth, G., Bunnenberg, E., and Djerassi, C. (1978) Magnetic circular dichroism of purified forms of rabbit liver cytochromes P-450 and P-420. *Biochemistry* **17,** 33–42
48. Dolinger, P. M., Kielczewski, M., Trudell, J. R., Barth, G., Linder, R. E., Bunnenberg, E., and Djerassi, C. (1974) Magnetic circular dichroism studies XXV. A preliminary investigation of microsomal cytochromes. *Proc. Natl. Acad. Sci. U.S.A.* **71,** 399–403
49. Shimizu, T., Iizuka, T., Mitani, F., Ishimura, Y., Nozawa, T., and Hatano, M. (1981) Magnetic and natural circular dichroism spectra of cytochrome *P*-450$_{11\beta}$ and *P*-450$_{SCC}$ purified from bovine adrenal cortex. *Biochim. Biophys. Acta* **669,** 46–59
50. Spiro, T. G., and Li, X.-Y. (1988) in *Resonance Raman Spectra of Heme and Metalloproteins* (Spiro, T. G., ed) pp. 1–38, 1st Ed., John Wiley & Sons, New York
51. Andersson, L. A., Mylrajan, M., Sullivan, E. P., Jr., and Strauss, S. H. (1989) Modeling low-pH hemoproteins. *J. Biol. Chem.* **264,** 19099–19102
52. Kitagawa, T., Kyogoku, Y., Iizuka, T., and Saito, M. I. (1976) Nature of the iron-ligand bond in ferrous low spin hemoproteins studied by resonance Raman scattering. *J. Am. Chem. Soc.* **98,** 5169–5173
53. Spiro, T. G., Soldatova, A. V., and Balakrishnan, G. (2013) CO, NO, and O_2 as vibrational probes of heme protein interactions. *Coord. Chem. Rev.* **257,** 511–527
54. Marvin, K. A., Reinking, J. L., Lee, A. J., Pardee, K., Krause, H. M., and Burstyn, J. N. (2009) Nuclear receptors *Homo sapiens* Rev-erbβ and *Drosophila melanogaster* E75 are thiolate-ligated heme proteins which undergo redox-mediated ligand switching and bind CO and NO. *Biochemistry* **48,** 7056–7071
55. Lazilotta, W. N., Schuller, D. J., Thorsteinsson, M. V., Kerby, R. L., Roberts,

G. P., and Poulos, T. L. (2000) Structure of the CO sensing transcription activator CooA. *Nat. Struc. Biol.* **7,** 876–880
56. Pardee, K. I., Xu, X., Reinking, J., Schuetz, A., Dong, A., Liu, S., Zhang, R., Tiefenbach, J., Lajoie, G., Plotnikov, A. N., Botchkarev, A., Krause, H. M., and Edwards, A. (2009) The structural basis of gas-responsive transcription by the human nuclear hormone receptor REV-ERBβ. *PLoS Biol.* **7,** e43
57. Reinking, J., Lam, M. M., Pardee, K., Sampson, H. M., Liu, S., Yang, P., Williams, S., White, W., Lajoie, G., Edwards, A., and Krause, H. M. (2005) The *Drosophila* nuclear receptor e75 contains heme and is gas responsive. *Cell* **122,** 195–207
58. Igarashi, J., Murase, M., Iizuka, A., Pichierri, F., Martinkova, M., and Shimizu, T. (2008) Elucidation of the heme-binding site of heme-regulated eukaryotic initiation factor 2α kinase and the role of the regulatory motif in heme sensing by spectroscopic and catalytic studies of mutant proteins. *J. Biol. Chem.* **283,** 18782–18791
59. Uchida, T., Sato, E., Sato, A., Sagami, I., Shimizu, T., and Kitagawa, T. (2005) CO-dependent activity-controlling mechanism of heme-containing CO-sensor protein, neuronal PAS domain protein 2. *J. Biol. Chem.* **280,** 21358–21368
60. Yin, L., Dragnea, V., and Bauer, C. E. (2012) PpsR, a regulator of heme and bacteriochlorophyll biosynthesis, is a heme-sensing protein. *J. Biol. Chem.* **287,** 13850–13858
61. Jones, D. T. (1999) Protein secondary structure prediction based on position-specific scoring matrices. *J. Mol. Biol.* **292,** 195–202
62. Nash, A. I., McNulty, R., Shillito, M. E., Swartz, T. E., Bogomolni, R. A., Luecke, H., and Gardner, K. H. (2011) Structural basis of photosensitivity in a bacterial light-oxygen-voltage/helix-turn-helix (LOV-HTH) DNA-binding protein. *Proc. Natl. Acad. Sci. U.S.A.* **108,** 9449–9454
63. Moran, L. A., Scrimgeour, K. G., Horton, H. R., Ochs, R. S., and Rawn, J. D. (1994) *Biochemistry*, 2nd Ed., p. 14.27, Neil Patterson/Prentice Hall, Englewood Cliffs, NJ
64. Mayhew, S. G. (1978) Redox potential of dithionite and $SO2-$ from equilibrium reactions with flavodoxins, methyl viologen and hydrogen plus hydrogenase. *Eur. J. Biochem.* **85,** 535–547
65. Chim, N., Johnson, P. M., and Goulding, C. W. (2014) Insights into redox sensing metalloproteins in *Mycobacterium tuberculosis*. *J. Inorg. Biochem.* **133,** 118–126
66. Aono, S., Ohkubo, K., Matsuo, T., and Nakajima, H. (1998) Redox-controlled ligand exchange of the heme in the CO-sensing transcriptional activator CooA. *J. Biol. Chem.* **273,** 25757–25764
67. Vogel, K. M., Spiro, T. G., Shelver, D., Thorsteinsson, M. V., and Roberts, G. P. (1999) Resonance Raman evidence for a novel charge relay activation mechanism of the CO-dependent heme protein transcription factor CooA. *Biochemistry* **38,** 2679–2687
68. Shimizu, T. (2012) Binding of cysteine thiolate to the Fe(III) heme complex is critical for the function of heme sensor proteins. *J. Inorg. Biochem.* **108,** 171–177
69. Yukl, E. T., Ioanoviciu, A., Nakano, M. M., de Montellano, P. R., and Moënne-Loccoz, P. (2008) A distal tyrosine residue is required for ligand discrimination in DevS from *Mycobacterium tuberculosis*. *Biochemistry* **47,** 12532–12539
70. Fan, B., Wang, J., Stuehr, D. J., and Rousseau, D. L. (1997) NO synthase isozymes have distinct substrate binding sites. *Biochemistry* **36,** 12600–12665
71. Li, D., Stuehr, D. J., Yeh, S.-R., and Rousseau, D. L. (2004) Heme distortion modulated by ligand-protein interactions in inducible nitric-oxide synthase. *J. Biol. Chem.* **279,** 26489–26499
72. Ibrahim, M., Xu, C., and Spiro, T. G. (2006) Differential sensing of protein influences by NO and CO vibrations in heme adducts. *J. Am. Chem. Soc.* **128,** 16834–16845
73. Vogel, K. M., Kozlowski, P. M., Zgierski, M. Z., and Spiro, T. G. (2000) Role of the axial ligand in heme-CO backbonding; DFT analysis of vibrational data. *Inorg. Chim. Acta* **297,** 11–17
74. Uchida, T., Ishikawa, H., Takahashi, S., Ishimori, K., Morishima, I., Ohkubo, K., Nakajima, H., and Aono, S. (1998) Heme environmental structure of CooA is modulated by the target DNA binding. Evidence from resonance Raman spectroscopy and CO rebinding kinetics. *J. Biol. Chem.* **273,** 19988–19992
75. Tomita, T., Gonzalez, G., Chang, A. L., Ikeda-Saito, M., and Gilles-Gonzalez, M. A. (2002) A comparative resonance Raman analysis of heme-binding PAS domains: Heme iron coordination structures of the *Bj*FixL, *Ax*PDEA1, *Ec*Dos, and *Mt*Dos proteins. *Biochemistry* **41,** 4819–4826
76. Walker, F. A. (1999) Magnetic spectroscopic (EPR, ESEEM, Mössbauer, MCD and NMR) studies of low-spin ferriheme centers and their corresponding heme proteins. *Coord. Chem. Rev.* **185,** 471–534

Supplementary Material to

Redox Dependent Ligand Switching in a Novel Sensory Heme-binding GAF Domain of the Photosynthetic Cyanobacteria *Nostoc* sp. PCC7120

Kun Tang[1,2], Markus Knipp[2,3], Bing-bing Liu[1], Nicholas Cox[2], Robert Stabel[2], Qi He[1], Ming Zhou[1], Hugo Scheer[4], Kai-hong Zhao[1,*], Wolfgang Gärtner[2,*]

From the [1]State Key Laboratory of Agricultural Microbiology, Huazhong Agricultural University, Wuhan 430070, P.R China and [2]Max Planck Institute for Chemical Energy Conversion, Stiftstr. 34-36, D-45470 Mülheim, Germany and [3]Resolv, Faculty for Chemistry and Biochemistry, Ruhr University Bochum, D-44780 Bochum, Germany and [4]Department Biologie I, Ludwig-Maximilians-Universität, Menzinger Str. 67, D-80638 München, Germany

Table S1: Primers for the cloning of wild-type gene and for site-directed mutagenesis; mutated nucleotides are given in red.

Primer	Sequence	DNA
P1	5'- ATACCATGGGGCCTATTTCTCTACATGATG -3' (*Nco*I)	pET28-*all4978*
P2	5'- AATCTCGAGTCGATGAATTAGCTGGTCTT -3' (*Xho*I)	
P3	5'- ATTCCATGGGCACAATTCCCCTAAAGCT -3' (*Nco*I)	pET28-*all7016*
P4	5'- ATACTCGAGTTGCTGGGAGTTCGGCACTA -3' (*Xho*I)	
P5	5'- GTCGGATCCATGCCTATTTCTCTACAT -3' (*BamH*I)	pET30- *all4978 (1-170)*
P6	5'- TTTGTCGACTTAAATTTGTAATTCGCG -3' (*Sal*I)	
P7	5'- CTAGAATTCCCCCTAAAGCTGATTTTT -3' (*EcoR*I)	pET30- *all7016 (4-168)*
P8	5'- CCAGTCGACTTAGCTTTGAAAAGGATA -3' (*Sal*I)	
P9	5'- CGCGAATTCATGTCTGTTACTTTACCAAC-3' (*EcoR*I)	pET30- *alr7522 (1-173)*
P10	5'- TGAGTCGACTTAGGGCACAAATAACTCG -3' (*Sa*lI)	
Mutagenesis primers for $GAF_{All4978}$		
P11	5'- GTGCAACATTGGGGCATCGGTTTAATAGATAGTGAATC -3'	**Y41G**
P12	5'- GATTCACTATCTATTAAACCGATGCCCCAATGTTGCAC -3'	
P13	5'- GTGCAACATTGGGGCATCTTTTTAATAGATAGTGAATC -3'	**Y41F**
P14	5'- GATTCACTATCTATTAAAAAGATGCCCCAATGTTGCAC -3'	
P15	5'- GAAGACTGGAAAGACTTCGGTCCACGCCACGACCAC -3'	**C92G**

P16	5’- GTGGTCGTGGCGTGGACCGAAGTCTTTCCAGTCTTC -3’	
P17	5’- GAAAGACTTCTGTCCACGCGGCGACCACGGACACGTCATG -3’	**H95G**
P18	5’- CATGACGTGTCCGTGGTCGCCGCGTGGACAGAAGTCTTTC -3’	
P19	5’- CTGTCCACGCCACGACGGCGGACACGTCATGACC -3’	**H97G**
P20	5’- GGTCATGACGTGTCCGCCGTCGTGGCGTGGACAG -3’	
P21	5’- CGCCACGACCACGGACACGTCATGA -3’	**C92S**
P22	5’- TGGGCTGAAGTCTTTCCAGTCTTCTGGGGTGAG -3’	
P23	5’- CATTTATCAGCCAAACTCGCCACCCTAAAA -3’	**C138S**
P24	5’- AATAGACAGGGCGCTGAGGTCGGCTAA -3’	
P25	5’- GGACACGTCATGACCGGGCCAATAATTTGC -3’	**H95A**
P26	5’- GTGGTCGGCGCGTGGACAGAAGTCTTTCC -3’	
P27	5’- GGACACGTCATGACCGGGCCAATAATTTGC -3’	**D96A**
P28	5’- GTGGGCGTGGCGTGGACAGAAGTCTTTCC -3’	
P29	5’- GGACACGTCATGACCGGGCCAATAATTTGC -3’	**H97A**
P30	5’- AGCGTCGTGGCGTGGACAGAAGTCTTTCC -3’	
P31	5’- GGAGCTGTCATGACCGGGCCAATAATTTGC -3’	**H99A**
P32	5’- GTGGTCGTGGCGTGGACAGAAGTCTTTCC -3’	

Redox-dependent Ligand Switching in a Sensory Heme-binding GAF Domain of the Cyanobacterium *Nostoc* sp. PCC7120

Kun Tang, Markus Knipp, Bing-Bing Liu, Nicholas Cox, Robert Stabel, Qi He, Ming Zhou, Hugo Scheer, Kai-Hong Zhao and Wolfgang Gärtner

J. Biol. Chem. 2015, 290:19067-19080.
doi: 10.1074/jbc.M115.654087 originally published online June 10, 2015